Risuteganib Protects against Hydroquinone–induced Injury in Human RPE Cells

Ping Yang,[1] Zixuan Shao,[2] Nicholas A. Besley,[1] Samantha E. Neal,[1] Kristen L. Buehne,[1] John Park,[2] Hampar Karageozian,[2] Vicken Karageozian,[2] Ian T. Ryde,[3] Joel N. Meyer,[3] and Glenn J. Jaffe[1]

[1]Department of Ophthalmology, Duke University Eye Center, Durham, North Carolina, United States
[2]Allegro Ophthalmics, LLC, San Juan Capistrano, California, United States
[3]Nicholas School of the Environment, Duke University, Durham, North Carolina, United States

Correspondence: Glenn J. Jaffe, Department of Ophthalmology, Duke University Medical Center, 2351 Erwin Road, Durham, NC 27710, USA; jaffe001@mc.duke.edu.

Received: March 6, 2020
Accepted: July 2, 2020
Published: August 20, 2020

Citation: Yang P, Shao Z, Besley NA, et al. Risuteganib protects against hydroquinone–induced injury in human RPE cells. *Invest Ophthalmol Vis Sci.* 2020;61(10):35. https://doi.org/10.1167/iovs.61.10.35

Purpose. Cigarette smoking has been implicated in the pathogenesis of AMD. Integrin dysfunctions have been associated with AMD. Herein, we investigate the effect of risuteganib (RSG), an integrin regulator, on RPE cell injury induced by hydroquinone (HQ), an important oxidant in cigarette smoke.

Methods. Cultured human RPE cells were treated with HQ in the presence or absence of RSG. Cell death, mitochondrial respiration, reactive oxygen species production, and mitochondrial membrane potential were measured by flow cytometry, XFe24 analyzer, and fluorescence plate reader, respectively. Whole transcriptome analysis and gene expression were analyzed by Illumina RNA sequencing and quantitative PCR, respectively. F-actin aggregation was visualized with phalloidin. Levels of heme oxygenase-1, P38, and heat shock protein 27 proteins were measured by Western blot.

Results. HQ induced necrosis and apoptosis, decreased mitochondrial bioenergetics, increased reactive oxygen species levels, decreased mitochondrial membrane potential, increased F-actin aggregates, and induced phosphorylation of P38 and heat shock protein 27. HQ, but not RSG alone, induced substantial transcriptome changes that were regulated by RSG cotreatment. RSG cotreatment significantly protected against HQ-induced necrosis and apoptosis, prevented HQ-reduced mitochondrial bioenergetics, decreased HQ-induced reactive oxygen species production, improved HQ-disrupted mitochondrial membrane potential, reduced F-actin aggregates, decreased phosphorylation of P38 and heat shock protein 27, and further upregulated HQ-induced heme oxygenase-1 protein levels.

Conclusions. RSG has no detectable adverse effects on healthy RPE cells, whereas RSG cotreatment protects against HQ-induced injury, mitochondrial dysfunction, and actin reorganization, suggesting a potential role for RSG therapy to treat retinal diseases such as AMD.

Keywords: AMD, RPE, Integrin, oxidative stress

RPE cells form a monolayer of highly specialized, polarized epithelial cells interposed between the choriocapillaris and photoreceptors. RPE cells play an important role in retinal homeostasis and are vital to photoreceptor cell health and visual function.[1]

RPE cell dysfunction or death is thought to be an important contributor to AMD.[2,3] RPE cells are continually exposed to oxidants throughout life and oxidative stress plays a major role in the pathogenesis and progression of AMD.[2,4] Cigarette smoke contains high concentrations of free oxidants and has been implicated as a major environmental risk factor for AMD.[3] Hydroquinone (HQ), a major oxidant in both tobacco smoke and atmospheric pollutants, increases reactive oxygen species (ROS) generation and promotes oxidative stress.[5] ROS, a group of unstable oxygen-containing molecules that can easily react with other molecules in a cell, are generated during cellular metabolism and in response to various stimuli. In cells, the major site of ROS production is the mitochondrial electron transport chain, where some electrons leak from the transport process and spontaneously react with molecular oxygen, producing superoxide anion.[6] ROS have important physiological functions; however, excess ROS can cause RPE cell oxidative damage.[4,7]

Mitochondria, the intracellular organelles comprising the main respiratory machinery in cells, are crucial for energy production and cell homeostasis. Owing to a high level of metabolic demand by photoreceptors, RPE cells are enriched with a large mitochondrial population to meet the high-energy needs. Consequently, RPE mitochondrial dysfunction can lead to tissue damage and has been implicated in the development of AMD.[8] In RPE cells from eyes with

AMD, damaged, fragmented, and ruptured mitochondria have been observed.[9] Mitochondrial DNA mutation levels are also elevated in RPE cells of eyes with AMD.[7,10,11]

Integrins, a family of heterodimeric, noncovalently bound cell adhesion proteins, are transmembrane receptors consisting of a larger α subunit and a smaller β subunit. Integrins serve as bridges between cells and regulate cellular interaction with other surrounding cells and with the extracellular matrix through signal transduction pathways.[12] Physiologically, they play important roles in cell adhesion, proliferation, shape, and motility. They are involved in a variety of biological processes, and are also central to the etiology and pathology of many disease states. Integrins $\alpha v\beta 3$, $\alpha v\beta 5$, and $\alpha 5\beta 1$, for example, are closely associated with choroidal neovascularization in eyes with wet AMD.[13,14] Therefore, integrins are an attractive target to treat retinal diseases.

Risuteganib (RSG; also known as Luminate, ALG-1001, Allegro Ophthalmics, LLC, San Juan Capistrano, CA) is an engineered arginylglycylaspartic acid class synthetic peptide that modulates integrin receptors. RGD peptide treatment suppresses retinal neovascularization and facilitates the release of cellular adhesion between the vitreous and the retina, inducing posterior vitreous detachment.[15,16] In previous studies, RSG decreased expression of several disease-relevant integrins, including $\alpha v\beta 3$, $\alpha v\beta 5$, $\alpha 2\beta 1$, and $\alpha 5\beta 1$[17,18] (Kaiser PK, et al. IOVS 2017;58:ARVO E-Abstract 2029), which are expressed in RPE cells.[19,20] Earlier studies also suggest a potential cytoprotective effect of RSG, which would be beneficial in retinal degenerative diseases such as dry AMD (Beltran MA, et al. IOVS 2018;59:ARVO E-Abstract 1465). The phase II clinical study of RSG in intermediate dry AMD demonstrated statistically significant improvements in visual acuity and a phase III study to determine the effects of RSG in intermediate dry AMD is currently planned.[21,22] However, there is minimal published information to directly address the protective role of RSG on RPE cells and the mechanisms by which the drug exerts its effect. Herein, we investigated the effect of RSG on HQ-induced RPE cell injury, in an in vitro cell culture system.

Methods

Reagents

RSG was obtained from Allegro Ophthalmics, LLC. HQ, the tetrazolium salt WST-1 (4-[3-(4-Iodophenyl)-2-(4-nitrophenyl)-2H-5-tetrazolio]-1.3-benzene disulfonate), phalloidin-TRITC (cat# P1951), and collagen type I were purchased from Sigma (St. Louis, MO). TrypLE (cat# 12604-013), Annexin V Pacific Blue conjugate (cat# A35122), Annexin V binding buffer (cat# V13246), eBioscience 7-AAD viability staining solution (cat# 00-6993-50), JC-1 dye and 5-(and-6)-chloromethyl-2',7'-dichlorodihydrofluorescein diacetate, acetyl ester (CM-H2DCFDA), BCA protein assay kit, radioimmunoprecipitation assay lysis and extraction buffer (cat# 89900), and TURBO DNA-free kit were purchased from Thermo Scientific (Chicago, IL). Cell mito stress test kit (cat# 103015-100), XF base medium (cat# 103193-100), and XFe24 FluxPak (cat# 102342-100) were purchased from Agilent technologies (Santa Clara, CA). RNeasy Mini and RNeasy Plus Mini Kits were purchased from Qiagen (Valencia, CA). Rabbit anti-heme oxygenase-1 (HO-1; cat# ADI-OSA-150D) antibody was purchased from Enzo Life Sciences (Farmingdale, NY). Rabbit anti-P38 (cat# 9212), rabbit anti-phospho-P38 (Thr180/Tyr182, D3F9, cat# 4511), mouse anti-heat shock protein 27 (HSP27; cat# 2402), and rabbit anti-phospho-HSP27 (Ser82, D1H2F6, cat# 9709) antibodies were purchased from Cell Signaling Technology (Danvers, MA). Mouse anti-GAPDH antibody was purchased from Chemicon (Temecula, CA).

Human RPE Cell Culture and Treatments

Human donor eyes from a 62-year-old male donor were obtained from the North Carolina Organ Donor and Eye Bank, Inc. (Winston-Salem, NC) in accordance with the provisions of the Declaration of Helsinki for research involving human tissue. RPE cells were collected as previously described.[23] Cells were grown in Eagle's minimal essential medium (MEM; Invitrogen) with 10% fetal bovine serum (Thermo Scientific) and with 1× penicillin/streptomycin (Thermo Scientific) at 37°C in a humidified environment containing 5% CO_2. The identity of RPE cells was confirmed by cytokeratin-18 and ZO-1 stain (not shown).

Human donor RPE cells were seeded on collagen-coated 96-well plates (0.8×10^4/well), 24-well plates with or without coverslips (6×10^4/well), 12-well plates (10×10^4/well), and 6-well plates (25×10^4/well) (Corning-Costar Incorporated, Corning, NY), as we have previously described.[24] Except for the Seahorse assay, on day 6 after plating, cells were washed twice with serum-free, phenol red-free MEM (SF-MEM), and treated with HQ at a various concentrations in the presence or absence of RSG (0.4 mM) in SF-MEM for various times at 37°C. Different doses of HQ were used in the following assays; the effects of HQ varied depending on the vessel in which they were plated. We observed that cells grown in 6-well plates were more resistant to HQ-induced damage when compared with those plated in 96-well plates, despite similar density per growth area. To compensate for these differential effects, we optimized the concentrations and exposure times for each assay to produce similar levels of oxidant injury, regardless of the plates used to grow the cells. Elsewhere in this article, RSG cotreatment refers to the condition in which cells were cotreated with RSG and HQ. Control refers to the condition in which cells were treated with SF-MEM alone.

Flow Cytometry

RPE cells in triplicate wells of a 6-well plate were treated with HQ (150 µM) in the presence or absence of RSG (0.4 mM) for 12 hours. Cell morphology was recorded by light microscopy, and then cells were detached with 1× TrypLE and centrifuged at 300*g* for 5 minutes. Cells were resuspended with 100 µL 1× Annexin V binding buffer, incubated with 5 µL Annexin V for 10 minutes and then 5 µL 7-AAD was added to the Annexin V mixture and incubated for additional 5 minutes. Cell death was analyzed with flow cytometry.

WST Assay

RPE cells in triplicate wells of a 96-well plate were treated with HQ (150 µM) for 2.5 hours in the presence or absence of RSG (0.4 mM). The medium was removed and cells were incubated with WST-1 solution for 30 minutes at 37°C. A colorimetric assay was performed based on the cleavage of the tetrazolium salt WST-1 by mitochondrial dehydrogenases in viable cells. The plate was read on a spectrophotometer at 440 nm with a reference wavelength at 690 nm.

Investigative Ophthalmology & Visual Science

Seahorse Assay

RPE cells were seeded in triplicate wells of collagen-coated XF 24-well plates and grown for 24 hours. RPE cells that had just reached confluence were washed with SF-MEM and treated for 1.5 hours with HQ (175 µM) with or without RSG (0.4 mM). Media were removed and cells were washed with XF base medium containing 1 mM sodium pyruvate, 2 mM glutamine, and 8 mM glucose at a pH of 7.4. The cells were incubated for 1 hour at 37°C in a CO_2-free incubator. The oxygen consumption rate (OCR) was measured by Seahorse XFe24 flux analyzer under basal conditions followed by the sequential addition of 1 µM oligomycin, 1 µM trifluorocarbonylcyanide phenylhydrazone, and 1 µM rotenone and antimycin A. Maximal OCR was the difference in OCR between trifluorocarbonylcyanide phenylhydrazone–induced respiration and OCR after injection of antimycin A. Mitochondrial spare respiratory capacity was the difference between maximal respiration and the basal OCR. Media were removed and the total proteins were extracted for BCA protein assay after OCR measurements. OCRs were normalized to the total protein content.

Determination of ROS

RPE cells in triplicate wells of 96-well black plates with clear bottoms were washed with SF-MEM, loaded with 20 µM CM-H2DCFDA in SF-MEM for 30 minutes at 37°C and then washed twice. Cells were then treated with HQ (160 µM) in the presence or absence of RSG (0.4 mM). Fluorescence was measured at various times with a fluorescence plate reader (490 nm excitation, 522 nm emission).

Determination of Mitochondrial Membrane Potential

RPE cells in triplicate wells of 96-well black plates with clear bottoms were washed with SF-MEM, loaded with 10 µM JC-1 dye in SF-MEM for 30 minutes at 37°C and then washed twice. Cells were then treated with HQ (160 µM) with or without RSG (0.4 mM). A fluorescence plate reader was used to measure the fluorescence at various times to quantify green JC-1 monomer (490 nm excitation, 522 nm emission) and red JC-1 aggregates (535 nm excitation, 590 nm emission).

RNA-sequencing (RNA-seq) Sample Preparation and Analysis

RPE cells in sextuplicate wells of a 6-well plate were treated for 4 hours with HQ (250 µM or 300 µM) in the presence or absence of RSG (0.4 mM). Total RNA was extracted using an RNeasy Mini Kit and DNA was removed with TURBO DNA-free kit. RNA quality was measured with a Bioanalyzer (Agilent Genomics, Santa Clara, CA). RNA-seq libraries were prepared from poly-A enriched messenger RNA and sequenced by GENEWIZ (South Plainfield, NJ) to generate approximately 20 to 30 million paired-end, 150 base pair reads per sample. RNA-seq FASTQ files were quality tested with FastQC.[25] Reads were aligned with STAR[26] to human genome (GRCh38.p12) and transcriptome (GENECODE v30) references, followed by read quantification with the featureCounts software.[27]

A principal component analysis was used to visualize the high-dimensional RNA-seq dataset using the top 15,000 genes that had the highest average counts, as normalized by DESeq2's VST method.[28] Differential expression analysis was performed using edgeR exact test[29]; analysis limited to genes with count per million of 1 or greater in at least six samples in the dataset (collectively referred to as expressed genes). Differentially expressed (DE) genes are defined to have a false discovery rate of less than 0.05 and an absolute value of a log2-fold-change absolute value of greater than 0.25. Strongly regulated DE genes, defined as those with an absolute value of a log2-fold-change absolute value of greater than 0.50, were submitted to goseq[30] for enrichment of gene ontology biological processes[31,32] and Kyoto Encyclopedia of Genes and Genomes[33] biological pathways that are overrepresented in the gene list. Biological processes and pathways were considered statistically significant with adjusted *P* values of less than 0.05. Enriched biological processes were condensed and visualized with REVIGO[34] with a similarity metric set to small and the gene ontology term size determined by Uniport *Homo Sapiens* database; biologically relevant processes were selected and labeled. Six enriched Kyoto Encyclopedia of Genes and Genomes pathways were selected for visualization of gene expression changes, based on their biological relevance and the strength of the negative correlation between HQ and RSG cotreatment. Empirical RNA-seq Sample Size Analysis (ERSSA)[35] was used to check whether the six biological replicates used in this study were sufficient for differential expression discovery; the analysis was performed with a log2-fold change cutoff of 0.25 and 50 subsamples at each replicate level.

Real-time RT-PCR Analysis

RPE cells in triplicate wells of a 12-well plate were treated for 4 hours with HQ (250 µM) in the presence or absence of RSG (0.4 mM). Total RNA was isolated using RNeasy Plus Mini Kit according to the manufacturer's specifications and real-time quantitative RT-PCR was performed as we have described previously.[36] Primer pairs for HMOX-1 and ribosomal protein, large, P0 (RPLP0) were as follows (5′ to 3′): *HMOX-1*, forward: CAG GAG CTG ACC CAT GA; reverse: AGC AAC TGT CGC CAC CAG AA; and *RPLP0*, forward: GGA CAT GTT GCT GGC CAA TAA; reverse: GGG CCC GAG ACC AGT GTT.

F-actin Immunofluorescent Staining

RPE cells in triplicate wells of a 24-well plate containing collagen-coated coverslips were treated for 6 hours with HQ (140 µM) in the presence or absence of RSG (0.4 mM) and then fixed in 4% paraformaldehyde for 12 minutes at room temperature. Cells were permeabilized with 0.5% Triton X-100 for 12 minutes and incubated for 1 hour at room temperature with phalloidin-TRITC in 0.5% bovine serum albumin/0.1% Triton X-100/PBS. The percentage of F-actin aggregates was determined by a masked observer. Briefly, for each sample, 10 to 11 Z-stack images (covering 12 μm at 1-μm z-steps, six along the *x*-axis and five along the *y*-axis nonoverlapping fields) were captured under identical conditions with a 20× objective on a Nikon A1 confocal microscope. Maximum intensity projected images were imported into Fiji open-source imaging software and segmented using the Trainable Weka Segmentation plugin following Fiji's online instructions. Briefly, for generation of a "threshold," a segmentation classifier was created using an image containing both aggregates and nonaggregates. Aggregates and nonaggregates were traced and added into separate groups, respectively. This process was repeated

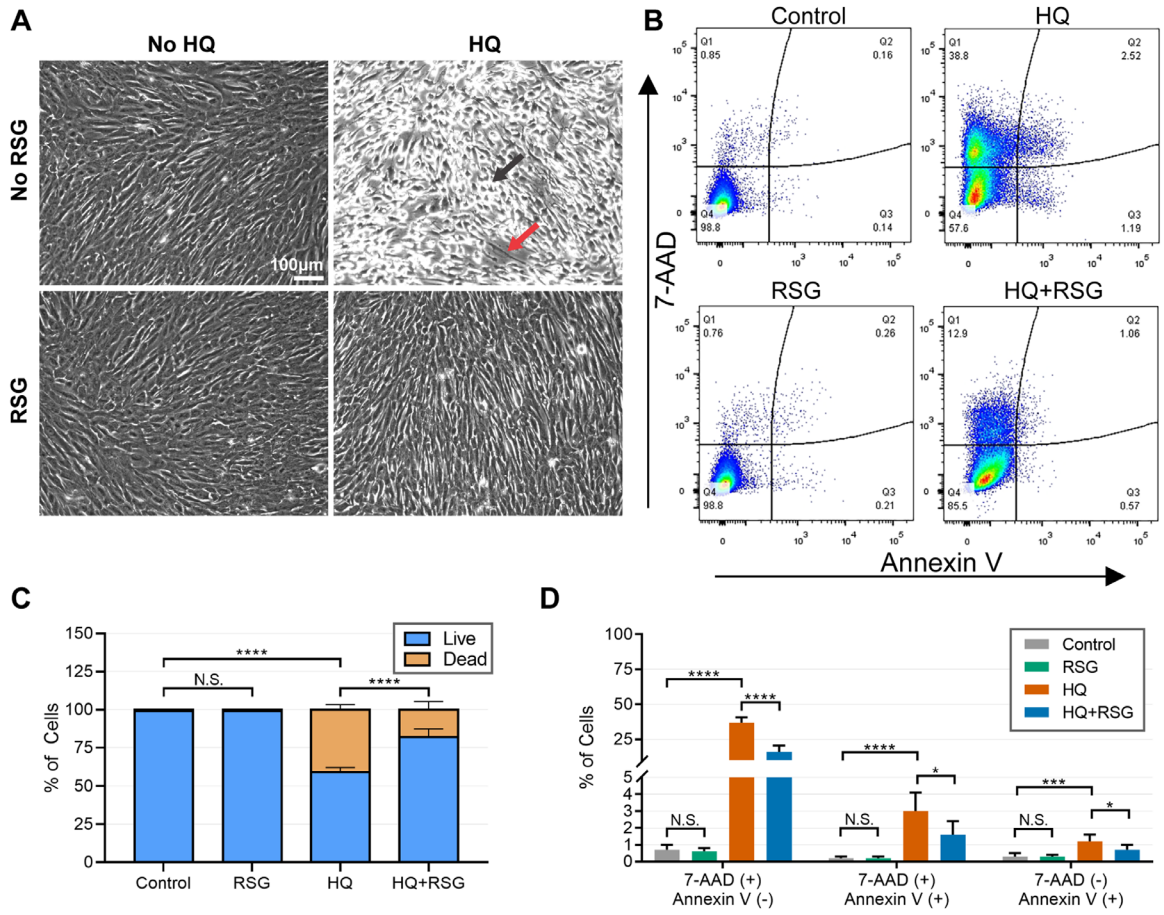

Figure 1. RSG cotreatment protected against HQ-mediated RPE cell death. RPE cells in triplicate wells of a 6-well plate were treated for 12 hours with HQ (150 μM) in the presence or absence of RSG. (**A**) Morphology of cells was captured before cell harvest. A large number of the HQ-treated RPE cells appeared less adherent (*black arrow*) and other cells seemed to be shriveled (*red arrow*). (**B–D**) Cells were then harvested and stained with Annexin V and 7-AAD. Cell death was analyzed with flow cytometry. HQ primarily induced RPE cell necrosis and to a lesser extent, apoptosis. RSG cotreatment significantly protected against both HQ-induced necrosis and apoptosis. Data were averaged from two separate experiments ($n = 6$ per condition).

until satisfactory image segmentation was achieved. The classifier was then tested on three images that had varying degrees of aggregate density to ensure accurate segmentation. For data analysis, segmented images were converted to eight-bit, binary images and F-actin aggregates were quantified using the particle analyzer function (0–infinity size and 0–1 circularity) in Fiji.

Western Blot

RPE cells in triplicate wells of 12-well or 6-well plates were treated for various times with HQ (160 μM in 12-well plates or 170 μM in 6-well plates) in the presence or absence of RSG (0.4 mM). Total protein was extracted with radioimmunoprecipitation assay buffer supplemented with protease inhibitors and phosphatase inhibitors, quantified with Bradford protein assay, and subjected to sodium dodecyl sulfate polyacrylamide gel electrophoresis and Western blot as we have previously described.[24]

Statistical Analysis

Data are expressed as the mean ± standard deviation. Two-way ANOVA with Tukey multiple comparisons correction was used to determine whether there were statistically significant differences between treatment groups as measured by flow cytometry, WST assay, XFe24 flux analyzer, ROS assay, JC-1 assay, F-actin aggregates analysis, quantitative RT-PCR, and Western blot. Results were plotted using GraphPad Prism 8.3.0 with asterisks indicating the magnitude of P value (N.S. = not significant, * $P \leq 0.05$, ** $P \leq 0.01$, *** $P \leq 0.001$, and **** $P \leq 0.0001$).

Results

RSG Cotreatment Protects against HQ-mediated RPE Cell Death

To investigate whether RSG protected against HQ-induced RPE cell death, flow cytometry analysis was performed with annexin V and 7-AAD staining to identify apoptosis and necrosis, respectively. Early apoptotic cells are Annexin V positive and 7-AAD negative. Late apoptotic cells are Annexin V and 7-AAD double positive. Necrotic cells are 7-AAD positive and Annexin V negative. As shown in Figure 1A, HQ (150 μM) caused cells to shrivel or detach, whereas RSG cotreatment improved HQ-induced morphologic changes. A similar morphology was observed in cells

Investigative Ophthalmology & Visual Science

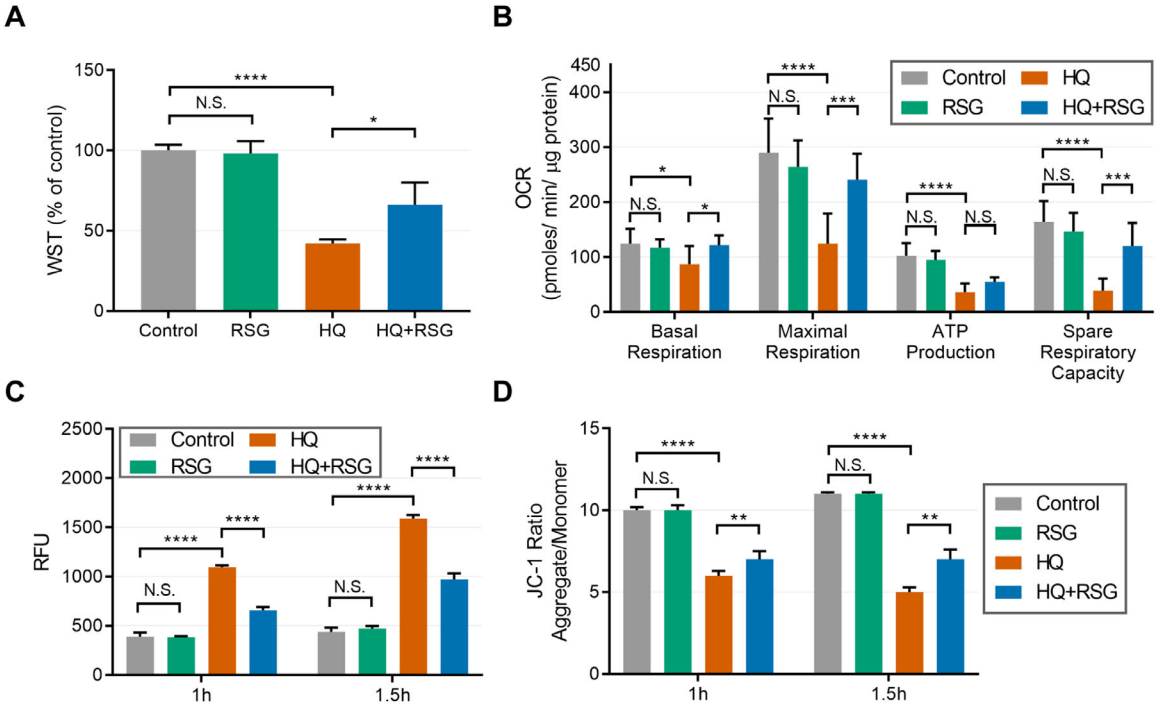

Figure 2. RSG cotreatment protected against the HQ-induced deleterious effect on mitochondrial function. (**A**) RPE cells in triplicate wells of a 96-well plate were treated for 2.5 hours with HQ (150 µM) in the presence or absence of RSG. Cell viability as reflected by mitochondrial dehydrogenase activity was measured with the WST-1 reagent. RSG cotreatment significantly protected cells from HQ-decreased cell viability. Data are representative of three separate experiments with similar results. (**B**) RPE cells in triplicate wells were treated for 1.5 hours with HQ (175 µM) in the presence or absence of RSG. Basal respiration, maximal OCR, ATP production, and spare respiratory capacity were significantly decreased in HQ-treated cells versus control, whereas RSG cotreatment significantly increased mitochondrial metabolic parameters when compared with HQ-treated cells. Data are averaged from three separate experiments ($n = 9$ per condition). (**C**) RPE cells in triplicate wells of a 96-well plate were loaded with 20 µM CM-H2DCFDA for 30 minutes and washed twice. Cells were treated with HQ (160 µM) in the presence or absence of RSG. ROS production was measured by relative fluorescence units (RFU) at the indicated times using a fluorescence plate reader. RSG cotreatment significantly decreased HQ-induced ROS generation. Data are representative of three separate experiments with similar results. (**D**) RPE cells in triplicate wells of a 96-well plate were loaded with 10 µM JC-1 dye for 30 minutes and washed twice. Cells were treated with HQ (160 µM) in the presence or absence of RSG. The $\Delta\Psi$m was measured at the indicated times by the fluorescence of JC-1 monomers and aggregates. RSG cotreatment significantly improved HQ-mediated reduction of $\Delta\Psi$m. Data are representative of three separate experiments with similar results.

treated with RSG alone, when compared with control. As shown in Figure 1B through D, HQ induced primarily necrotic cell death and much less apoptotic cell death. RSG cotreatment significantly protected cells from HQ-induced necrosis and apoptosis. RSG alone had little effect on the number of live and dead cells compared with control.

RSG Cotreatment Protects Cells from Deleterious Effects of HQ on Mitochondria

WST-1 is a stable tetrazolium salt that can be cleaved by cellular mitochondrial dehydrogenase to form a soluble formazan. The amount of formazan generated by mitochondrial dehydrogenase activity is directly proportional to the number of living cells, which makes it useful as a cell viability assay. Accordingly, to further evaluate RSG's cytoprotective effect, a WST assay was performed. As shown in Figure 2A, HQ significantly decreased cell viability as reflected by decreased mitochondrial dehydrogenase activity when compared with control, while RSG cotreatment significantly increased HQ-reduced cell viability. RSG alone had little effect on cell viability when compared with control.

To evaluate the role of RSG in the regulation of mitochondrial function, we measured mitochondrial respiration. HQ significantly decreased mitochondrial bioenergetics when compared with control. RSG cotreatment significantly increased basal respiration, maximal respiration, and spare respiratory capacity when compared with HQ-treated cells. No significant change in mitochondrial bioenergetics was detected in cells treated with RSG alone, when compared with control (Fig. 2B).

To examine whether RSG decreases oxidative stress-mediated ROS production, we measured ROS levels. As shown in Figure 2C, ROS production was significantly increased in HQ-treated cells when compared with control, whereas RSG cotreatment significantly decreased HQ-induced ROS production. RSG alone did not significantly change ROS level when compared with control.

Mitochondrial membrane potential ($\Delta\Psi$m) is critical to maintain the physiological function of the respiratory chain to generate ATP. The membrane-permeant JC-1 dye is widely used to test $\Delta\Psi$m. To evaluate the effect of RSG on HQ-mediated changes in $\Delta\Psi$m, we determined the ratio of JC-1 monomers to aggregates. As shown in Figure 2D, the $\Delta\Psi$m was significantly decreased in HQ-treated cells when compared with control, whereas RSG cotreatment

Investigative Ophthalmology & Visual Science

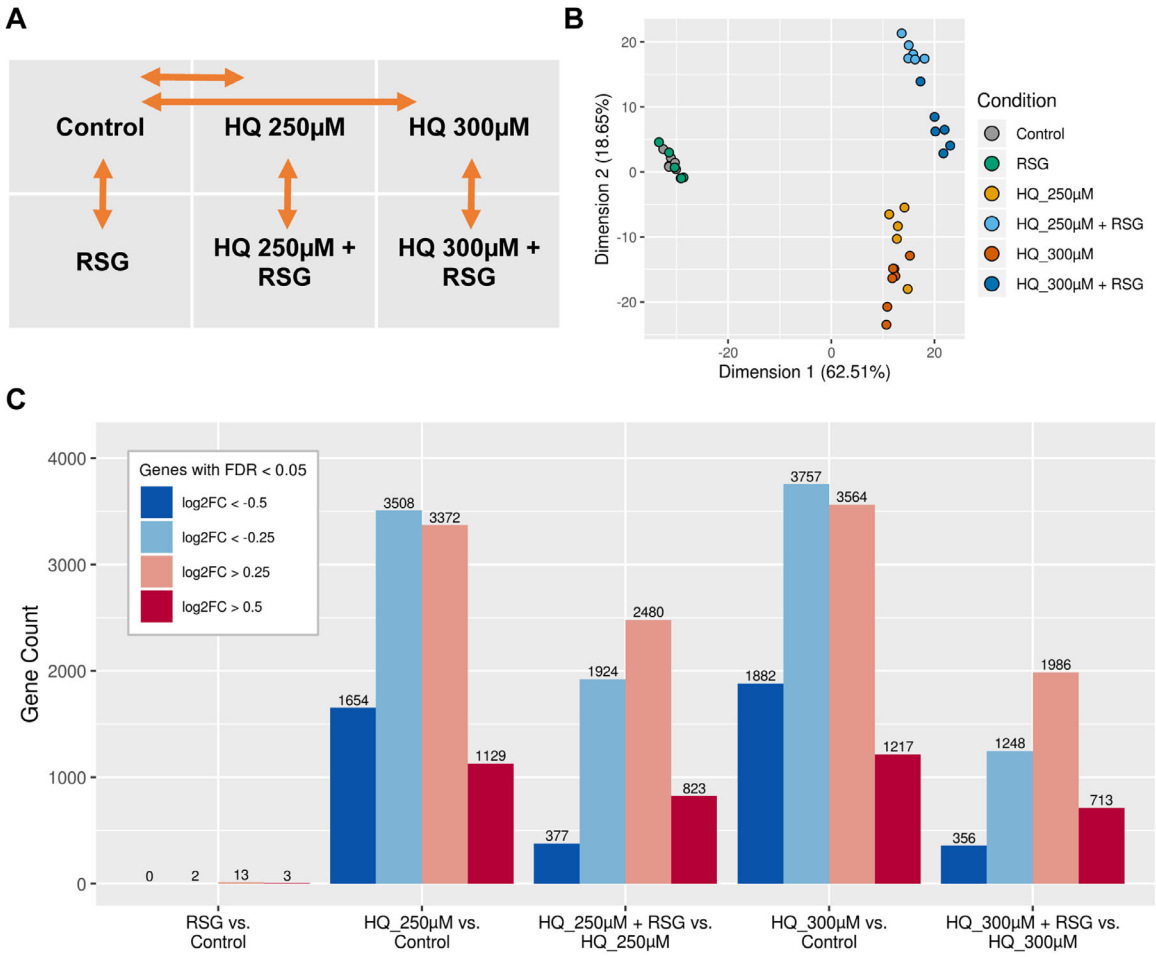

Figure 3. HQ and RSG cotreatment-initiated gene expression changes. RPE cells in sextuplicate wells of 6-well plate were treated for 4 hours with HQ at 250 μM or 300 μM in the presence or absence of RSG. Poly-A–enriched messenger RNAs were isolated and sequenced using RNA-seq. (**A**) The six treatment conditions. *Orange arrows* indicate the differential expression comparisons performed. (**B**) A principal component analysis was used to visualize the samples on the first two dimensions that captured the largest amount of variance (shown in axis label) in the dataset. First two dimensions showed clear separation between control, HQ-treated, and RSG cotreated cells. (**C**) The edgeR software was used to identify genes that are DE between selected conditions. The number of genes that passed the false discovery rate and log2-fold change thresholds are shown. The number of genes that were strongly downregulated, downregulated, upregulated, or strongly upregulated are colored in *dark blue*, *blue*, *red*, or *dark red*, respectively. Few DE genes were found after RSG treatment alone, whereas HQ treatment and RSG cotreatment induced large transcriptome changes.

significantly improved the HQ-mediated decrease in the ΔΨm. When compared with control, RSG alone did not induce significant changes in the ΔΨm.

RSG Cotreatment Modulates HQ-regulated Transcriptome

To investigate gene expression changes in response to HQ and RSG, RPE cells were exposed for 4 hours to HQ at two dosages (250 μM or 300 μM) with or without RSG, followed by whole transcriptome measurement using RNA-seq (Fig. 3A). All RNA-seq samples had excellent RNA quality (Bioanalyzer RNA Integrity Number > 9.70) and sequencing quality (data not shown). Principal component analysis visualization of the samples showed that the top two dimensions captured a combined 81% of variance in the dataset and revealed clear separation on dimension 1 between HQ-treated and nontreated cells and on dimension 2 between HQ-treated and RSG cotreated cells. No observable separation was discovered between cells treated with RSG alone and control (Fig. 3B).

On differential expression analysis, approximately 7000 genes were changed in HQ-treated cells at the two dosages tested when compared with control, whereas RSG treatment alone only changed 15 DE genes (Fig. 3C, Supplementary Fig. S1). However, compared with cells treated with HQ alone, RSG cotreatment also regulated thousands of genes. Further analysis showed that many of the genes influenced by RSG cotreatment were also regulated by HQ and the expression frequently changed in the opposite direction to that induced by HQ (Fig. 4A: HQ 250 μM, 2017 of 4404 or 46% of genes; Supplementary Fig. S2A: HQ 300 μM, 1165 of 3234 or 36% of genes). Additionally, when all HQ-regulated genes were evaluated, negative correlations were observed between expression changes modulated by HQ and RSG cotreatment (Fig. 4B: HQ 250 μM, –0.2166; Supplementary Fig. S2B: HQ 300 μM, –0.1039), indicating that RSG modulates HQ-induced expression changes.

Investigative Ophthalmology & Visual Science

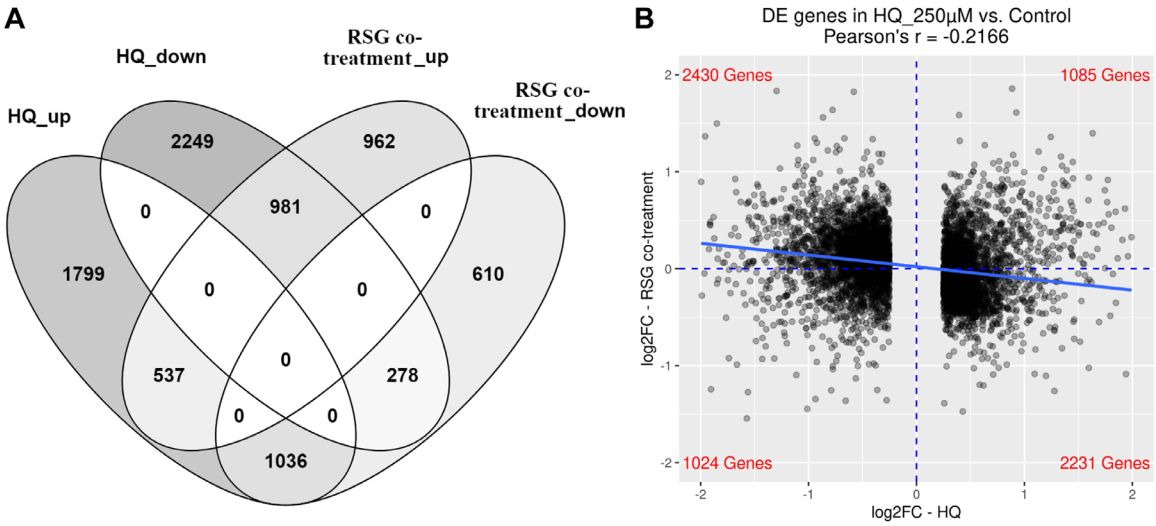

Figure 4. RSG cotreatment suppressed HQ-regulated gene expression. RNA-seq measured gene expression similarities and differences between RPE cells treated with HQ at 250µM (HQ_250µM vs. control) versus RSG cotreatment (HQ_250µM + RSG vs. HQ_250µM). (**A**) A Venn diagram represents the DE genes affected by HQ and RSG cotreatment, separated by direction of expression change. Shades of *gray* represent number of genes. A large proportion of RSG cotreatment-regulated genes showed expression change opposite in direction to that of HQ. (**B**) Visualization of a log2-fold change of DE genes in HQ_250 µM versus control. The *x*-axis represents the gene's log2-fold change in the HQ comparison, and the *y*-axis represents the corresponding log2-fold change in the RSG cotreatment comparison. The display is limited to a (−2, 2) range on both axes and is divided into four quadrants by $x = 0$ and $y = 0$ lines shown in blue dotted lines; labels in *red* indicate the number of genes in each quadrant. Linear regression of data is shown as a *solid blue line*. A moderately negative correlation was observed between gene expression changes associated with HQ and RSG cotreatment.

A functional analysis of the DE gene lists was performed to identify biological processes and pathways that are significantly enriched in genes regulated by HQ, RSG treatment alone, or RSG cotreatment. Among the 15 DE genes found regulated by RSG treatment alone, no processes or pathways were enriched. When performed with genes regulated by either HQ or RSG cotreatment, a large number of processes were enriched, including cell proliferation, cell death, regulation of cell adhesion, regulation of metabolism, inflammatory response, and response to stimulus (Fig. 5A, B: HQ 250 µM; Supplementary Fig. S3A, B: HQ 300 µM). In particular, a large number of processes overlapped between the two analyses (HQ 250 µM: 489 of 747 or 65% of processes enriched with RSG cotreatment-regulated genes; HQ 300 µM: 428 of 774 or 55% of processes enriched with RSG cotreatment-regulated genes), indicating that many of the same biological processes are regulated by HQ and RSG cotreatment. Similarly, enriched biological pathways showed large overlap between HQ and RSG cotreatment, including cytokine and cytokine receptor interaction, mitogen-activated protein kinase (MAPK), Janus kinase-signal transducer and activator of transcription (JAK-STAT), and TGF-β signaling (Fig. 5C, D: HQ 250 µM; Supplementary Fig. S3C, D: HQ 300 µM). Although many of the same biologically relevant pathways were regulated by HQ and RSG cotreatment, their induced changes were generally in opposite directions as indicated by the negative correlations (Fig. 5E: HQ 250 µM; Supplementary Fig. S3E: HQ 300 µM). Overall, gene expression changes across the two dosages of HQ tested by RNA-seq were highly consistent as shown by the large positive correlations (Supplementary Fig. S4).

For the five differential expression comparisons tested, RNA-seq sample size analysis was performed using ERSSA. Briefly, ERSSA determines if sufficient biological replicates have been used to discover a majority of DE genes in any specific comparison. ERSSA showed that sufficient samples were used in four of the comparisons to produce meaningful numbers of DE genes, as the average discovery trends tapered off when sample size approached $n = 6$, the number of biological replicates per condition in this experiment. In the comparison of RSG versus control, ERSSA showed that additional replicates were unlikely to further improve discovery beyond low double-digit number of DE genes (Supplementary Fig. S5).

RSG Cotreatment Decreases HQ-induced F-actin Aggregation, P38 MAPK Activation, and HSP27 Phosphorylation

The RNA-seq analysis suggested that RSG cotreatment regulated genes in a variety of oxidant-induced pathways, including those that affect actin cytoskeleton (Fig. 5E, Supplementary S3E). Oxidant-induced cytoskeleton reorganization to form F-actin aggregates reflects a deleterious effect on RPE cells.[37] To further explore the functional effects of RSG on F-actin injury during oxidative stress, cells were treated with HQ with or without RSG, and then F-actin aggregates were quantified. HQ significantly increased the number of F-actin aggregates when compared with control, whereas RSG cotreatment significantly inhibited the production of HQ-induced aggregates. RSG alone had no observable effect on F-actin cytoskeleton morphology and no significant change in number of F-actin aggregates when compared with control (Figs. 6A, B).

RNA-seq data showed that MAPK pathway genes were modulated by HQ alone and RSG cotreatment (Fig. 5C, Supplementary S3C, D). P38 MAPK activation is associated with F-actin aggregation in ARPE-19 cells.[37] To support a role for the MAPK pathway on the observed RSG effects on

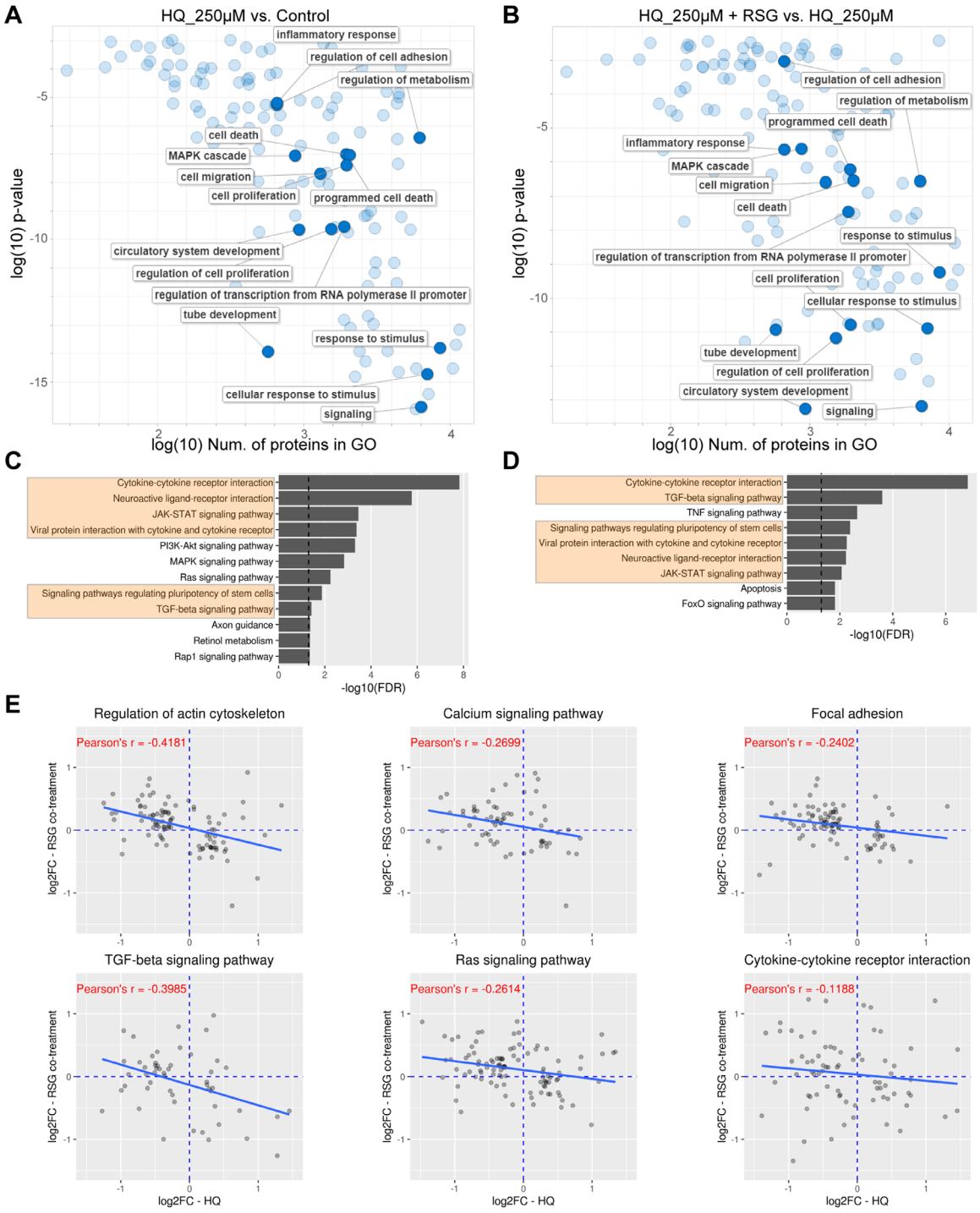

Figure 5. Biological processes and pathways regulated by HQ and RSG cotreatment. Biological processes (**A**, **B**) and pathways (**C**, **D**) enriched with DE genes regulated by HQ (HQ_250μM vs. control, **A** and **C**) and RSG cotreatment (HQ_250μM + RSG vs. HQ_250μM, **B** and **D**). (**A**, **B**) Enriched biological processes are summarized and displayed; selected biologically relevant processes are labeled. Many processes were regulated by both HQ and RSG cotreatment. (**C**, **D**) Enriched biological pathways are ranked by the false discovery rate with a dotted line at the false discovery rate of 0.05. Many pathways were regulated by both HQ and RSG cotreatment as shown in *orange* highlight. (**E**) Visualization of the log2-fold change of DE genes from selected biological pathways enriched with DE genes regulated by HQ or RSG cotreatment. The *x*-axis represents the gene's log2-fold change in the HQ comparison, and the *y*-axis represents the corresponding log2-fold change in the RSG cotreatment comparison. The display is limited to a (−1.5, 1.5) range on both axes. Linear regression of data is shown as *solid blue lines*. Across biologically relevant pathways, negative correlations were observed between expression changes associated with HQ and RSG cotreatment.

Investigative Ophthalmology & Visual Science

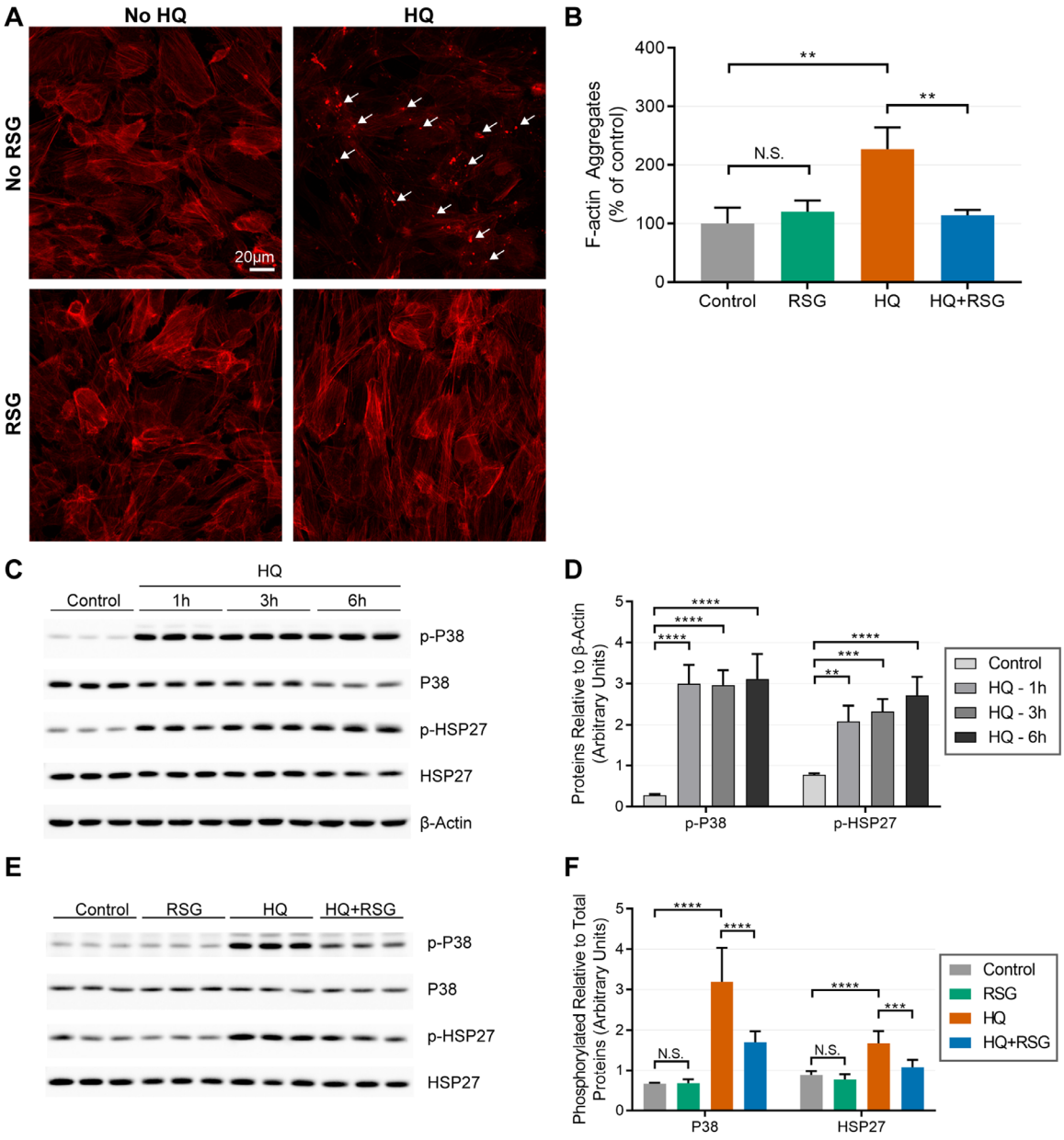

Figure 6. RSG cotreatment decreased HQ-induced F-actin aggregations, P38 activation and HSP27 phosphorylation. (**A, B**) RPE cells in triplicate wells of a 24-well plate containing coverslips were treated for 6 hours with HQ (140 μM) in the presence or absence of RSG and then stained with phalloidin-TRITC. (**A**) HQ induced F-actin aggregation (*white arrows*). (**B**) F-actin aggregates were quantified with Fiji Image-J. HQ significantly induced RPE F-actin aggregation versus control, while RSG cotreatment significantly decreased HQ-induced aggregation. Data are representative of three separate experiments with similar results. (**C-F**) RPE cells in triplicate wells of a 12-well plate were treated for either indicated times (**C-D**) or 1 hour (**E-F**) with HQ (160 μM) in the presence or absence of RSG. Total proteins (30 μg) were separated by sodium dodecyl sulfate polyacrylamide gel electrophoresis for Western blot (**C, E**). (**D**) The quantity of proteins relative to β-actin indicated that HQ induced P38 activation and HSP27 phosphorylation. Data are representative of three separate experiments with similar results. (**E**) The quantity of phosphorylated proteins relative to total proteins indicated that RSG cotreatment decreased P38 activation and HSP27 phosphorylation. Data were averaged from two separate experiments ($n = 6$ per condition).

F-actin aggregation, we performed Western blots to investigate whether RSG cotreatment affected P38 MAPK activation and phosphorylation of HSP27, an important P38 substrate. We first conducted time-course assays to evaluate the peak time of HQ-induced P38 activation for subsequent RSG cotreatment studies. We found that HQ significantly increased P38 phosphorylation 20 minutes after treatment (data not shown), which increased further by 1 hour, and was then maintained for at least 6 hours (Figs. 6C, D). Accordingly, we chose the 1-hour time point for RSG cotreatment experiments. We found that RSG cotreatment significantly decreased HQ-induced P38 activation and HSP27 phosphorylation 1 hour after treatment (Figs. 6E, F).

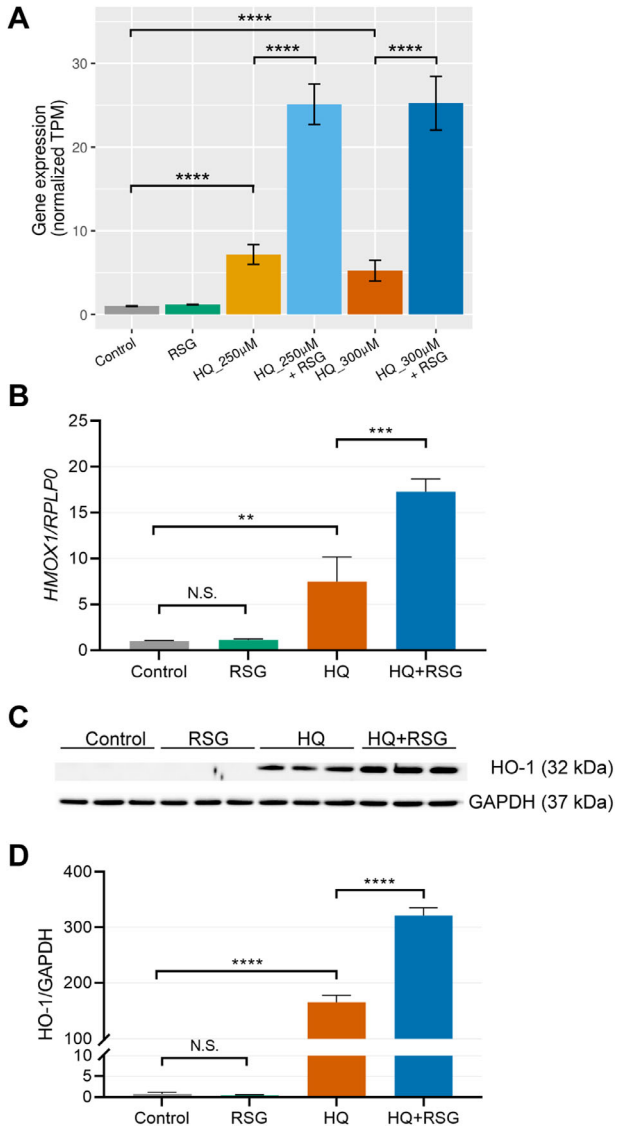

Figure 7. RSG cotreatment upregulated HQ-induced HO-1 expression. (**A, B**) RPE cells were treated for 4 hours with HQ (250 μM) in the presence or absence of RSG. RNA was extracted and gene expression was analyzed via RNA-seq (**A**) and quantitative RT-PCR (**B**). RSG cotreatment upregulated HQ-induced *HMOX-1* gene expression. (**C-D**) RPE cells in triplicate wells of a 6-well plate were treated for 8 hours with HQ (170 μM) in the presence or absence of RSG. Total proteins (30 μg) were separated by sodium dodecyl sulfate polyacrylamide gel electrophoresis for Western blot (**C**). (**D**) The quantity of HO-1 relative to GAPDH indicated that HQ-elevated HO-1 protein level was further upregulated by RSG cotreatment. Data are representative of two separate experiments with similar results.

RSG Cotreatment Upregulates HQ-induced HO-1 Expression

RNA-seq data indicated that HQ exposure strongly upregulated the cytoprotective *HMOX-1* gene that encodes HO-1 protein (618% and 420% increase by 250 μM and 300 μM HQ, respectively), which was further enhanced by RSG cotreatment (241% and 391% increase, respectively) when compared with expression levels induced by 250 μM and 300 μM HQ alone (Fig. 7A).

To confirm the RNA-seq results, *HMOX-1* gene expression and HO-1 protein levels were examined by quantitative RT-PCR and Western blot, respectively. As shown in Figures 7B–D, the *HMOX-1* gene and HO-1 protein levels were significantly upregulated by HQ and further upregulated by RSG cotreatment.

Discussion

In this study, we demonstrated that RSG treatment alone had no detectable adverse effect on healthy cells, whereas RSG cotreatment significantly (1) protected against HQ-induced RPE cell necrosis and apoptosis, (2) improved HQ-induced cell viability reduction, (3) prevented HQ-decreased mitochondrial bioenergetics, (4) suppressed HQ-induced ROS production, and (5) improved HQ-disrupted $\Delta\Psi m$. Furthermore, RSG alone minimally affected the RPE cell transcriptome, whereas HQ induced substantial transcriptome changes. RSG cotreatment modified many of these HQ-regulated biological processes and pathways. RSG cotreatment mitigated F-actin aggregates and decreased HQ-induced P38 activation and HSP27 phosphorylation. *HMOX-1* mRNA and HO-1 protein levels were significantly upregulated by HQ and further upregulated by RSG cotreatment.

There is accumulating evidence to indicate that, in AMD, oxidative stress plays a critical role to cause RPE cell dysfunction and death.[38] The mechanism by which oxidative stress induces RPE death in this disease is still controversial. Most in vitro studies indicate that oxidative stress induces primarily apoptotic cell death, although some studies suggest that necrosis contributes to RPE death.[39,40] Caspase 3/7 activity, measured as an apoptosis marker, is not changed in ARPE-19 cells after treatment with various HQ concentrations (50–500 μM) (Woo GB, et al. IOVS 2012;53:ARVO E-abstract 4276). In contrast, HQ downregulates apoptosis-related genes after HQ injury in differentiated ARPE-19 cells.[41] In the current study, we found that HQ primarily induced necrosis and, to a much lesser extent, apoptosis. RSG cotreatment significantly protected against both necrosis and apoptosis induced by HQ. Integrins trigger a variety of cell signaling cascades that have profound effects on cell viability. Integrins also play a complex role to regulate cell survival, and their dysfunction can lead to apoptosis.[42] Our results suggest that RSG plays a role to protect against oxidative stress-induced integrin-mediated RPE necrosis and apoptosis.

It is well-known that apoptosis is a highly regulated process. However, a significant component of necrotic death also occurs through highly regulated mechanisms.[43] Necrosis can include signs of controlled processes, such as mitochondrial dysfunction, enhanced generation of ROS, adenosine triphosphate depletion, and plasma membrane failure.[44] Thus, mitochondrial dysfunction plays an important role in both apoptosis and necrosis.[45,46] HQ increases ROS levels and decreases the $\Delta\Psi m$ in ARPE-19 cells.[47] The results obtained from donor RPE in the current study were consistent with data from ARPE-19 cells. In Seahorse assays, we found that HQ significantly decreased mitochondrial basal respiration, maximal respiration, adenosine triphosphate production, and spare respiratory capacity. RSG cotreatment significantly protected cells from the deleterious effects of HQ on mitochondrial bioenergetics. These observations of mitochondrial protection are consistent with studies of RSG in human Müller cells and ARPE-19 cells. (Kenney CM, et al. IOVS 2018;59:ARVO E-Abstract 771; Beltran MA, et al. IOVS 2018;59:ARVO E-Abstract 1465). Owing to the

important role mitochondria play in cellular function, integrin signaling can have a profound impact on the mitochondria and vice versa. Integrins control mitochondrial function and ROS production by interacting with small G proteins.[48] Integrin ligations trigger ROS production by promoting changes in mitochondrial metabolic/redox function[48] and activation of distinct oxidases.[49] Conversely, disruption of mitochondrial function with inhibitors increases ROS production and upregulates integrin $\beta 5$ expression in human gastric cancer SC-M1 cells.[50] Our results suggest that RSG, as an integrin regulator, can positively influence mitochondrial function, although integrin-independent effects cannot be ruled out.

RNA-seq is a powerful quantitative tool to explore genome-wide expression. To further investigate the therapeutic mechanism of action of RSG, we used RNA-seq as an unbiased method to assess the transcriptome changes induced by the HQ and RSG cotreatment. We found that RSG alone had minimal influence on the transcriptome, consistent with its limited effect on healthy RPE cells. A large transcriptome change involving roughly one-half of the detectable expressed genes was seen after HQ treatment. These observations are supported by our pathway analysis that showed regulation of genes in (1) inflammation pathways that included cytokine–cytokine receptor interaction and JAK-STAT signaling pathways, (2) cell proliferation and death pathways such as phosphoinositide-3-kinase–Akt, MAPK, TGF-β, and Ras signaling pathways, (3) cell adhesion and migration pathways such as focal adhesion and actin cytoskeleton regulation, and (4) pathways that function in diverse signaling systems such as the calcium signaling pathway. These findings are consistent with studies in various cell models that show regulation of cell growth, cell death, extracellular matrix, and stress response genes after HQ exposure.[41,51,52]

Although RSG alone elicited minimal transcriptome changes, RSG cotreatment significantly modified the cellular gene expression response to HQ stress. A significant portion of the RSG cotreatment-regulated genes were also regulated by HQ treatment alone, except the expression changes were in the opposite direction. Similarly, a functional analysis of RSG cotreatment-regulated genes indicated that they are involved in biological processes and pathways modulated by HQ. Taken together, these observations, which were consistent across two HQ dosages tested, suggest that RSG cotreatment moderated cellular transcriptome changes elicited by HQ.[53,54]

Actin cytoskeleton serves mechanical, organizational, and signaling roles that contribute to cellular functions. The regulation of the F-actin cytoskeleton depends on a variety of molecular mechanisms.[55] Oxidative stress is a key mechanism that causes aggregation of a number of proteins implicated in neurodegenerative disorders.[55,56] HQ induces F-actin aggregation through the phosphorylation of the P38/HSP27 cascade in ARPE-19 cells.[37] In the current study, we found that HQ also induced F-actin aggregation, P38 activation, and HSP27 phosphorylation in donor RPE cells, and RSG cotreatment abrogated these effects. These data complement the previous work in ARPE-19 cells[37] and provide a mechanistic explanation for the effect of RSG to inhibit F-actin aggregation. Actin cytoskeletal signaling networks are composed of a large group of proteins such as integrins, kinases, and small GTPases. Integrins can affect the actin cytoskeleton through a number of molecular linkages.[57,58] Integrins can either stimulate or suppress actin-based structures, indicating the variety of pathways leading from integrins to the cytoskeleton. A variety of studies demonstrate the functional link between integrin and P38. For example, blocking functionality or downregulation of αv integrin decreases endogenous P38 activation in breast cancer cells.[59] Our data indicate that there is a link between integrin regulation and P38 activation in human RPE cells and support the hypothesis that RSG prevents HQ-induced damage to normal actin cytoskeleton, at least in part by reversing the adverse effects of HQ on integrin regulated F-actin assembly.

The expression of HO-1 protein is highly upregulated by a variety of stress sources, including oxidative stress, substrate heme, ultraviolet light, hyperthermia, heavy metals, peroxides, endotoxins, and cytokines.[60,61] HO-1 induction is recognized as a pivotal cellular adaptive and protective response against oxidative stress toxicity.[62] *HMOX-1* mRNA levels are significantly increased in undifferentiated and differentiated ARPE-19 cells treated with t-butyl hydroperoxide and hydrogen peroxide,[63] whereas HO-1 protein expression is upregulated in ARPE-19 cells treated with cigarette smoke extract.[64] ARPE-19 cells that overexpress HO-1 are more resistant to t-butyl hydroperoxide–induced cell death[65] and HO-1 activation has shown to play an important role to protect against retinal injury.[66–69] In this study, *HMOX-1* was one of genes most upregulated by HQ and RSG cotreatment, which prompted us to further assess the effects on HO-1 protein levels. We found that *HMOX-1* gene and HO-1 protein expression were significantly upregulated by HQ and further increased by RSG cotreatment. Additional upregulation of HO-1 by RSG cotreatment beyond that induced by HQ alone suggests that RSG triggers the activation of antioxidant enzyme in response to oxidative stress to prevent HQ-induced cell death. However, activation of HO-1 was only observed when cells were under HQ stress, while RSG alone did not induce observable cellular stress and HO-1 activation. Further studies are needed to investigate the precise upstream molecular regulator of HO-1 activation[70] induced by HQ and RSG cotreatment.

Ultimately, any model, whether in vitro, or in vivo, cannot fully replicate human pathophysiology or response to treatment. However, such models are useful to gain insight into possible biochemical or disease mechanisms, and potential human therapeutic effects. HQ-induced RPE cell damage has been used as a model for oxidant injury in a variety of in vitro and in vivo studies.[71,72] Furthermore, many of these studies have used these models to explore a possible role of oxidants in AMD.[71,72] Detailed in vivo experiments with RSG are beyond the scope of the current report. However, existing data from animal studies indicate that RSG induces expression of antioxidant proteins, including superoxide dismutase, glutathione peroxidase, and catalase in corneal epithelium, which may contribute to RSG protection against desiccating stress-induced corneal damage in a dry eye mouse model (Quiroz-Mercado H, et al. IOVS 2019;60:ARVO E-Abstract 288). Our data demonstrate a protective role of RSG against oxidant injury and mitochondrial damage. This information complements the recent positive phase II clinical data that suggested RSG may be useful to treat intermediate AMD[21,22] and are consistent with the hypothesis that these observed therapeutic effects of RSG in intermediate AMD, at least in part, are mediated through its protective effects on oxidant injury. Furthermore, recent in vitro, in vivo, and clinical data suggest that another agent, elamipretide, that protects against mitochondrial injury, may

have a beneficial effect on AMD (Kapphahn R, et al. IOVS 2017;58:ARVO E-Abstract 1954; Cousins SW, et al. IOVS 2016; 57:ARVO E-Abstract 2126; Cousins SW, et al. IOVS 2019;60:ARVO E-Abstract 974). Taken together, these data, our RSG in vitro data, and RSG animal model and human clinical data support the hypothesis that oxidant injury is important in AMD pathogenesis and that agents to protect against oxidant injury may be useful therapeutic agents.

In conclusion, RSG cotreatment protects RPE cells against HQ-induced injury, restores mitochondrial function, and modifies a variety of the biological processes induced by HQ. Although some of these observations can be explained by the regulation of integrin by RSG, the precise molecular mechanisms governing the promotion of cell survival by RSG remain to be fully elucidated. We continue to investigate the RSG-modulated biological pathways and believe this information will enhance our understanding of a potential role for RSG therapy to treat degenerative retinal diseases, such as dry AMD.

Acknowledgments

Supported by NIH P30EY005722 (Core grant) and Research to Prevent Blindness.

Disclosure: **P. Yang**, None; **Z. Shao**, Allegro Ophthalmics, LLC (E); **N.A. Besley**, None; **S.E. Neal**, None; **K.L. Buehne**, None; **J. Park**, Allegro Ophthalmics, LLC (E); **H. Karageozian**, Allegro Ophthalmics, LLC (E); **V. Karageozian**, Allegro Ophthalmics, LLC (E); **I.T. Ryde**, None; **J.N. Meyer**, None; **G.J. Jaffe**, None

References

1. Kevany BM, Palczewski K. Phagocytosis of retinal rod and cone photoreceptors. *Physiology*. 2010;25:8–15.
2. Handa JT, Bowes Rickman C, Dick AD, et al. A systems biology approach towards understanding and treating non-neovascular age-related macular degeneration. *Nat Commun*. 2019;10:3347.
3. van Lookeren Campagne M, LeCouter J, Yaspan BL, Ye W. Mechanisms of age-related macular degeneration and therapeutic opportunities. *J Pathol*. 2014;232:151–164.
4. Beatty S, Koh H, Phil M, Henson D, Boulton M. The role of oxidative stress in the pathogenesis of age-related macular degeneration. *Surv Ophthalmol*. 2000;45:115–134.
5. Enguita FJ, Leitao, AL. Hydroquinone: environmental pollution, toxicity, and microbial answers. *Biomed Res Int*. 2013;2013:542168.
6. Birben E, Sahiner UM, Sackesen C, Erzurum S, Kalayci O. Oxidative stress and antioxidant defense. *World Allergy Org J*. 2012;5:9–19.
7. Karunadharma PP, Nordgaard CL, Olsen TW, Ferrington DA. Mitochondrial DNA damage as a potential mechanism for age-related macular degeneration. *Invest Ophthalmol Vis Sci*. 2010;51:5470–5479.
8. Kaarniranta K, Pawlowska E, Szczepanska J, Jablkowska A, Blasiak J. Role of mitochondrial DNA damage in ROS-mediated pathogenesis of age-related macular degeneration (AMD). *Int J Mol Sci*. 2019;20:2374.
9. Feher J, Kovacs I, Artico M, Cavallotti C, Papale A, Balacco Gabrieli C. Mitochondrial alterations of retinal pigment epithelium in age-related macular degeneration. *Neurobiol Aging*. 2006;27:983–993.
10. Lin H, Xu H, Liang FQ, et al. Mitochondrial DNA damage and repair in RPE associated with aging and age-related macular degeneration. *Invest Ophthalmol Vis Sci*. 2011; 52:3521–3529.
11. Terluk MR, Kapphahn RJ, Soukup LM, et al. Investigating mitochondria as a target for treating age-related macular degeneration. *J Neurosci*. 2015;35:7304–7311.
12. Barczyk M, Carracedo S, Gullberg D. Integrins. *Cell Tissue Res*. 2010;339:269–280.
13. Friedlander M, Theesfeld CL, Sugita M, et al. Involvement of integrins alpha v beta 3 and alpha v beta 5 in ocular neovascular diseases. *Proc Natl Acad Sci U S A*. 1996;93: 9764–9769.
14. Ramakrishnan V, Bhaskar V, Law DA, et al. Preclinical evaluation of an anti-alpha5beta1 integrin antibody as a novel anti-angiogenic agent. *J Exp Ther Oncol*. 2006;5:273–286.
15. Oliveira LB, Meyer CH, Kumar J, et al. RGD peptide-assisted vitrectomy to facilitate induction of a posterior vitreous detachment: a new principle in pharmacological vitreolysis. *Curr Eye Res*. 2002;25:333–340.
16. Yasukawa T, Hoffmann S, Eichler W, Friedrichs U, Wang YS, Wiedemann P. Inhibition of experimental choroidal neovascularization in rats by an alpha(v)-integrin antagonist. *Curr Eye Res*. 2004;28:359–366.
17. Kupperman B. A dual-mechanism drug for vitreoretinal diseases. *Retina Today*. July/August 2015;85–87.
18. Ishikawa M, Jin D, Sawada Y, Abe S, Yoshitomi T. Future therapies of wet age-related macular degeneration. *J Ophthalmol*. 2015;2015:138070.
19. Zarbin MA. Analysis of retinal pigment epithelium integrin expression and adhesion to aged submacular human Bruch's membrane. *Trans Am Ophthalmol Soc*. 2003;101:499–520.
20. Proulx S, Landreville S, Guerin SL, Salesse C. Integrin alpha5 expression by the ARPE-19 cell line: comparison with primary RPE cultures and effect of growth medium on the alpha5 gene promoter strength. *Exp Eye Res*. 2004;79:157–165.
21. Shaw LT, Mackin A, Shah R, et al. Risuteganib—a novel integrin inhibitor for the treatment of non-exudative (dry) age-related macular degeneration and diabetic macular edema. *Expert Opin Invest Drugs*. 2020;13:1–7.
22. Kuppermann BD. Risuteganib for intermediate dry AMD. Available at: wwwretinalphysiciancom/issues/2019/november-2019/risuteganib-for-intermediate-dry-amd. Accessed November 2019.
23. Jaffe GJ, Earnest K, Fulcher S, Lui GM, Houston LL. Antitransferrin receptor immunotoxin inhibits proliferating human retinal pigment epithelial cells. *Arch Ophthalmol*. 1990;108:1163–1168.
24. Yang P, Skiba NP, Tewkesbury GM, Treboschi VM, Baciu P, Jaffe GJ. Complement-mediated regulation of apolipoprotein E in cultured human RPE cells. *Invest Ophthalmol Vis Sci*. 2017;58:3073–3085.
25. Andrews S, FastQC A. A quality control tool for high throughput sequence data. Available at: www.bioinformatics.babraham.ac.uk/projects/fastqc/. 2010.
26. Dobin A, Davis CA, Schlesinger F, et al. STAR: ultrafast universal RNA-seq aligner. *Bioinformatics*. 2013;29:15–21.
27. Liao Y, Smyth GK, Shi W. featureCounts: an efficient general purpose program for assigning sequence reads to genomic features. *Bioinformatics*. 2014;30:923–930.
28. Love MI, Huber W, Anders S. Moderated estimation of fold change and dispersion for RNA-seq data with DESeq2. *Genome Biol*. 2014;15:550.
29. Robinson MD, McCarthy DJ, Smyth GK. edgeR: a Bioconductor package for differential expression analysis of digital gene expression data. *Bioinformatics*. 2010;26:139–140.
30. Young MD, Wakefield MJ, Smyth GK, Oshlack A. Gene ontology analysis for RNA-seq: accounting for selection bias. *Genome Biol*. 2010;11:R14.

Investigative Ophthalmology & Visual Science

31. Ashburner M, Ball CA, Blake JA, et al. Gene ontology: tool for the unification of biology. The Gene Ontology Consortium. *Nat Genet*. 2000;25:25–29.
32. The Gene Ontology Consortium. The Gene Ontology Resource: 20 years and still GOing strong. *Nucleic Acids Res*. 2018;47:D330–D338.
33. Ogata H, Goto S, Sato K, Fujibuchi W, Bono H, Kanehisa M. KEGG: Kyoto Encyclopedia of Genes and Genomes. *Nucleic Acids Res*. 1999;27:29–34.
34. Supek F, Bosnjak M, Skunca N, Smuc T. REVIGO summarizes and visualizes long lists of gene ontology terms. *PloS One*. 2011;6:e21800.
35. Shao Z. ERSSA: empirical RNA-seq sample size analysis. R package version 1.4.0. Available at: https://github.com/zshao1/ERSSA. 2019.
36. Yang P, Wiser JL, Peairs JJ, et al. Human RPE expression of cell survival factors. *Invest Ophthalmol Vis Sci*. 2005;46:1755–1764.
37. Pons M, Cousins SW, Csaky KG, Striker G, Marin-Castano ME. Cigarette smoke-related hydroquinone induces filamentous actin reorganization and heat shock protein 27 phosphorylation through p38 and extracellular signal-regulated kinase 1/2 in retinal pigment epithelium: implications for age-related macular degeneration. *Am J Pathol*. 2010;177:1198–1213.
38. Datta S, Cano M, Ebrahimi K, Wang L, Handa JT. The impact of oxidative stress and inflammation on RPE degeneration in non-neovascular AMD. *Prog Retin Eye Res*. 2017;60:201–218.
39. Hanus J, Zhang H, Wang Z, Liu Q, Zhou Q, Wang S. Induction of necrotic cell death by oxidative stress in retinal pigment epithelial cells. *Cell Death Dis*. 2013;4:e965.
40. Hanus J, Anderson C, Wang S. RPE necroptosis in response to oxidative stress and in AMD. *Ageing Res Rev*. 2015;24:286–298.
41. Strunnikova N, Zhang C, Teichberg D, et al. Survival of retinal pigment epithelium after exposure to prolonged oxidative injury: a detailed gene expression and cellular analysis. *Invest Ophthalmol Vis Sci*. 2004;45:3767–3777.
42. Stupack DG. Integrins as a distinct subtype of dependence receptors. *Cell Death Differ*. 2005;12:1021–1030.
43. Whelan RS, Konstantinidis K, Wei AC, et al. Bax regulates primary necrosis through mitochondrial dynamics. *Proc Natl Acad Sci U S A*. 2012;109:6566–6571.
44. Golstein P, Kroemer G. Cell death by necrosis: towards a molecular definition. *Trends Biochem Sci*. 2007;32:37–43.
45. Karch J, Molkentin JD. Regulated necrotic cell death: the passive aggressive side of Bax and Bak. *Circ Res*. 2015;116:1800–1809.
46. Baines CP. Role of the mitochondrion in programmed necrosis. *Front Physiol*. 2010;1:156.
47. Moustafa MT, Ramirez C, Schneider K, et al. Protective effects of memantine on hydroquinone-treated human retinal pigment epithelium cells and human retinal Muller cells. *J Ocul Pharmacol Ther*. 2017;33:610–619.
48. Werner E, Werb Z. Integrins engage mitochondrial function for signal transduction by a mechanism dependent on Rho GTPases. *J Cell Biol*. 2002;158:357–368.
49. Honore S, Kovacic H, Pichard V, Briand C, Rognoni JB. Alpha2beta1-integrin signaling by itself controls G1/S transition in a human adenocarcinoma cell line (Caco-2): implication of NADPH oxidase-dependent production of ROS. *Exp Cell Res*. 2003;285:59–71.
50. Hung WY, Huang KH, Wu CW, et al. Mitochondrial dysfunction promotes cell migration via reactive oxygen species-enhanced beta5-integrin expression in human gastric cancer SC-M1 cells. *Biochim Biophys Acta*. 2012;1820:1102–1110.
51. Sarma SN, Kim Y-J, Ryu J-C. Differential gene expression profiles of human leukemia cell lines exposed to benzene and its metabolites. *Environm Toxicol Pharmacol*. 2011;32:285–295.
52. Yang X, Lu Y, He F, et al. Benzene metabolite hydroquinone promotes DNA homologous recombination repair via the NF-kappaB pathway. *Carcinogenesis*. 2019;40:1021–1030.
53. Kaiser PK. Anti-integrin therapy in treatment of DME. http://retinatoday.com/2017/08/anti-integrin-therapy-in-treatment-of-dme/. *Retina Today*. July/August 2017;57–59.
54. Kaiser PK, Boyer DS, Campochiaro PA, et al. Topline results from prospective, double-masked, placebo controlled phase 2b clinical study evaluating Luminate® in patients with diabetic macular edema. *Invest Ophthalmol Vis Sci*. 2017;58:2029–2029.
55. Wilson C, Terman JR, Gonzalez-Billault C, Ahmed G. Actin filaments-A target for redox regulation. *Cytoskeleton (Hoboken)*. 2016;73:577–595.
56. Gardiner J, Overall R, Marc J. The nervous system cytoskeleton under oxidative stress. *Diseases*. 2013;1:36–50.
57. Calderwood DA, Shattil SJ, Ginsberg MH. Integrins and actin filaments: reciprocal regulation of cell adhesion and signaling. *J Biol Chem*. 2000;275:22607–22610.
58. Delon I, Brown NH. Integrins and the actin cytoskeleton. *Curr Opin Cell Biol*. 2007;19:43–50.
59. Chen J, Baskerville C, Han Q, Pan ZK, Huang S. αv integrin, p38 mitogen-activated protein kinase, and urokinase plasminogen activator are functionally linked in invasive breast cancer cells. *J Biol Chem*. 2001;276:47901–47905.
60. Baglole CJ, Sime PJ, Phipps RP. Cigarette smoke-induced expression of heme oxygenase-1 in human lung fibroblasts is regulated by intracellular glutathione. *Am J Physiol Lung Cell Mol Physiol*. 2008;295:L624–L636.
61. Loboda A, Damulewicz M, Pyza E, Jozkowicz A, Dulak J. Role of Nrf2/HO-1 system in development, oxidative stress response and diseases: an evolutionarily conserved mechanism. *Cell Mol Life Sci*. 2016;73:3221–3247.
62. Gozzelino R, Jeney V, Soares MP. Mechanisms of cell protection by heme oxygenase-1. *Annu Rev Pharmacol Toxicol*. 2010;50:323–354.
63. Alizadeh M, Wada M, Gelfman CM, Handa JT, Hjelmeland LM. Downregulation of differentiation specific gene expression by oxidative stress in ARPE-19 cells. *Invest Ophthalmol Vis Sci*. 2001;42:2706–2713.
64. Bertram KM, Baglole CJ, Phipps RP, Libby RT. Molecular regulation of cigarette smoke induced-oxidative stress in human retinal pigment epithelial cells: implications for age-related macular degeneration. *Am J Physiol Cell Physiol*. 2009;297:C1200–C1210.
65. Johnson J, Maher P, Hanneken A. The flavonoid, eriodictyol, induces long-term protection in ARPE-19 cells through its effects on Nrf2 activation and phase 2 gene expression. *Invest Ophthalmol Vis Sci*. 2009;50:2398–2406.
66. He M, Pan H, Chang RC, So KF, Brecha NC, Pu M. Activation of the Nrf2/HO-1 antioxidant pathway contributes to the protective effects of Lycium barbarum polysaccharides in the rodent retina after ischemia-reperfusion-induced damage. *PloS One*. 2014;9:e84800.
67. Orhan C, Akdemir F, Tuzcu M, et al. Mesozeaxanthin protects retina from oxidative stress in a rat model. *J Ocul Pharmacol Ther*. 2016;32:631–637.
68. Sun Y, Xiu C, Liu W, Tao Y, Wang J, Qu YI. Grape seed proanthocyanidin extract protects the retina against early diabetic injury by activating the Nrf2 pathway. *Exp Ther Med*. 2016;11:1253–1258.
69. Biswal MR, Justis BD, Han P, et al. Daily zeaxanthin supplementation prevents atrophy of the retinal pigment

Investigative Ophthalmology & Visual Science

epithelium (RPE) in a mouse model of mitochondrial oxidative stress. *PloS One*. 2018;13:e0203816.

70. Alam J, Cook JL. How many transcription factors does it take to turn on the heme oxygenase-1 gene? *Am J Respir Cell Mol Biol*. 2007;36:166–174.
71. Alcazar O, Hawkridge AM, Collier TS, et al. Proteomics characterization of cell membrane blebs in human retinal pigment epithelium cells. *Mol Cell Proteomics*. 2009;8:2201–2211.
72. Espinosa-Heidmann DG, Suner IJ, Catanuto P, Hernandez EP, Marin-Castano ME, Cousins SW. Cigarette smoke–related oxidants and the development of sub-RPE deposits in an experimental animal model of dry AMD. *Invest Ophthalmol Vis Sci*. 2006;47:729–737.